

Electronic structure, cohesive properties and magnetism of SrRuO₃; a theoretical investigation

Oscar Grånäs, Igor Di Marco, Olle Eriksson, Lars Nordström, and Corina Etz
Department of Physics and Astronomy, University of Uppsala

(Dated: July 31, 2022)

We have performed an extensive test of the ability of density functional theory within several approximations for the exchange-correlation functional, local density approximation+Hubbard U and local density approximation + dynamic mean field theory to describe magnetic and electronic properties of SrRuO₃. We focus on the ferromagnetic phase, illustrating differences between the orthorhombic low temperature structure vs the cubic high temperature structure. We assess how magnetism, spectral function, and cohesive properties are affected by methodology, on-site Hubbard U and double counting corrections. Further, we compare the impact of the impurity solver on the quasiparticle weight Z , which is in turn compared to experimental results. The spectral functions resulting from the different treatments are also compared to experimental data. The impact of spin-orbit coupling is also studied, allowing us to determine the orbital moments. In the orthorhombic phase the orbital moments are found to be tilted with respect to the spin moments, emphasising the importance of taking into account the distortion of the oxygen octahedra.

I. INTRODUCTION

The ruthenates have been the object of various experimental and theoretical investigations. This interest is stimulated by the fact that the layered ruthenates exhibit an impressive list of exotic phenomena. For example Sr₃Ru₂O₇ where meta-magnetism is known to occur¹, Sr₂RuO₄ with unusual p -wave superconductivity^{2,3} or long-range ferromagnetic order (rare in $4d$ -based materials) in SrRuO₃. The latter is a versatile compound whose properties can be drastically changed by doping or strain. For example Ca doping on the Sr sites leads to a poor metal, possibly non-Fermi-liquid behaviour, with no trace of magnetism⁴, while doping Cu on the Ru sites creates an insulating spin glass⁵. The double-perovskite Sr₂RuYO₆ has basically the same crystal structure as SrRuO₃ but one obtains an antiferromagnetic configuration by substituting every second Ru in Sr₂RuYO₆ with Y (Ref. 6). Hence the ferromagnetic state is unstable under small changes in the electronic structure, but still robust in the temperature range below ≈ 160 K. Also, intrinsic defects such as Ru vacancies are shown to have a big impact on magnetic properties⁷. It also shows an anomalously high magnetic anisotropy energy for an almost cubic material^{6,8}. Besides varied and interesting properties, the ruthenates are also good candidates for oxide electronics⁹, either alone or in combination with other complex oxides (e.g. in superlattices¹⁰). Even more, the hypothesis that SrRuO₃ might support the existence of magnetic monopoles in k -space¹¹ has been formulated.

Experimental measurements of the magnetic moment vary from $0.86 \mu_B$ to $1.6 \mu_B$, from e.g. Refs. 8 and 12, showing the delicate nature of the magnetic state. This large variation has been attributed to the difficulty of saturating the moment, due in part to the anomalously high magnetic anisotropy and in part to the challenging task of synthesising single domain structures¹³. One cannot neglect the dependence of the magnetic properties on the

sample quality.

Examining results from electronic structure calculations one also sees a variety of moments ranging from 0.5 - $2.0 \mu_B$ /Ru atom^{14,15}. In order to give a correct description of the properties of SrRuO₃, several computational tools have been applied. These include LDA/GGA^{6,13}, LDA+ U ¹⁵, pseudo-SIC¹³, GWA + LDA+ U ¹⁶ and recently LDA+DMFT¹⁴. One may observe from previous studies that the DFT description of SrRuO₃ strongly varies with respect to the (i) type of exchange-correlation (E_{xc}) functional used or (ii) the way these functionals are implemented. The main controversy about SrRuO₃ is the role of strong correlation in various properties. Infrared conductivity hints of non-fermi liquid properties¹⁷ and enhanced effective mass is detected in various experiments¹⁸⁻²⁰. Yet many properties seems to be well described within Kohn-Sham density functional theory, including only single Slater determinant physics, although very sensitive to the choice of exchange-correlation functional used. The DFT+SIC (self interaction correction) treatment of SrRuO₃ has proven to introduce an unphysical localisation of the Ru $4d$ states, leading to half-metallicity and too high moments, approaching the results given by DFT+ U , in the limit of large Hubbard U . With a more sophisticated method, such as LDA+ dynamical mean field theory (DMFT), it becomes interesting to investigate in detail the electronic structure and the effect of on-site correlations in SrRuO₃. Indeed, for the cubic phase of SrRuO₃ such an investigation has been reported, which highlights the importance of on-site correlation effects, however not driven by the proximity to the Mott insulator, but instead by the Hund's coupling^{21,22}.

The present study is focused on the investigation of the electronic structure and magnetic properties of SrRuO₃, both in the cubic and orthorhombic phase, by means of first principles DFT-based methods, in a full-potential geometry with emphasis on a many-body approach to correlated systems, i.e. the DMFT^{23,24}. In contrast to

previous LDA+DMFT studies¹⁴ we employ a full potential electronic structure method,²⁵ in which the first implementation of LDA+DMFT was reported in Ref. 26, with full charge self consistency using a recently developed implementation²⁷. The purpose of this study is to evaluate what method is most suitable for working with SrRuO₃ and related compounds. In order to achieve our aim, we compare the calculated quantities with experimentally measured data, such as magnetic moments, effective masses and photoemission spectra assessing the sensitivity to exchange correlation within DFT, followed by accurate full-charge self-consistent LDA+DMFT calculations, where U is varied within a reasonable range. In this way we make a critical assessment of the method that describes most accurately the properties of the SrRuO₃.

II. METHODOLOGY

The DFT implementation used here employs a full-potential geometry and a Linearized Muffin-Tin Orbitals (LMTO) basis set, as implemented in the RSPt-code^{25,28,29}. For the DFT part of the calculations we treat the narrow semi-core bands with a double κ -basis set. The s -, p - and d -valence bands are treated with a triple κ -basis. To assess that the quality of the DMFT results is not affected by the reduced basis, tests with double κ -basis are also performed for all volumes. The LDA+DMFT calculations are run with a double κ -basis in order to reduce the matrix dimensions and speed up the calculation. We perform calculations for SRO in both the cubic and orthorhombic phases. The Brillouin zone sampling for the orthorhombic phase is converged with respect to the equilibrium volume, magnetic moment, bulk modulus, spectral function and quasiparticle weights at $12 \times 12 \times 8$ k -points. The effects of spin-orbit interaction are more delicate and did not show convergence with a mesh of less than $24 \times 24 \times 16$ k -points (in order to ensure convergence, meshes up to $30 \times 30 \times 24$ k -points were considered). The cubic phase is converged at a mesh of $24 \times 24 \times 24$ k -points. For the DFT calculations we used the tetrahedron method with Blöchl's corrections³⁰ for integrations. As a starting point for the LDA+DMFT calculation we use the parametrization by von Barth and Hedin (vBH72). The final result will of course be somewhat dependent on the starting point. The LDA+DMFT is implemented in the Matsubara formalism^{26,27}, hence Fermi smearing is implicit. An electronic temperature of 110 K is used. We test five commonly used exchange-correlation functionals (E_{xc}), the LDA parametrizations by von Barth and Hedin (vBH72)³¹, Perdew and Wang (PW91)³² and Perdew and Zunger (PZ81)³³ as well as the GGA parametrizations by Armiento and Mattsson (AM05)³⁴ and Perdew, Burke and Enzerhof (PBE96)³⁵.

The impurity problem in the LDA+DMFT scheme is solved using the spin-polarized T-matrix fluctuation exchange solver (SPTF)³⁶. Two versions are tested, one where the diagrams are calculated with the unperturbed

Green's function (G_0) and one where the perturbation expansion is performed with a partially renormalized Green's function (G_{HF}) which consistently shows improvement in the description of magnetic properties³⁷. The SPTF solver, based on the fluctuation exchange (FLEX) approximation³⁸, works in the weak to intermediate coupling regime, demanding $U/W < 1$. The total 4d-bandwidth of SrRuO₃ is over ≈ 12 eV, with a distinct feature of a significantly narrower t_{2g} -band pinned at the Fermi level. The U values considered do not overcome 4 eV, and therefore we are in the regime where the FLEX solver is valid. As double counting we remove the static part of the self-energy³⁹. We also calculate the spectral properties and magnetic moments using LDA+ U , testing both the fully localized limit (FLL) and the around mean field (AMF) double countings. The strength of the Coulomb interaction parameter U on the d -electrons is varied between 2 eV and 4 eV, whereas J is set to 0.6 eV according to constrained random phase approximation calculations on Ru by Sasioglu et. al⁴⁰.

III. RESULTS

The phase diagram of SrRuO₃ shows that for temperatures up to 825 K the compound is present in the orthorhombic structure, with a ferromagnetic order that prevails up to $T_c = 160$ K. In the temperature range $825 < T < 945$, the crystal is tetragonal and becomes cubic for temperatures above 945 K. In the following, we focus on the orthorhombic phase, while making comparisons to the cubic phase with ferro magnetic arrangement of magnetic moments. In this way, we wish to determine and highlight the effect of the octahedral distortions and tilting on the properties of SrRuO₃. The experiments show no sign of ferromagnetism present in the cubic phase, although they indicate that local moments persist above T_c (Ref. 41) and these moments are most likely to contribute significantly to the physical properties of the cubic phase.

The orthorhombic cell is described according to recent neutron diffraction experiments by Bushmeleva et. al⁴². Their experiments show almost equal bond distances of ≈ 1.986 Å for all independent Ru-O bonds. This indicates the absence of Jahn-Teller distortions in the RuO₆ octahedra, confirming a low-spin state of the Ru⁴⁺ ion. The two independent Ru-O-Ru angles remain close to 162° for the whole temperature range between $1.5\text{K} < T < 290\text{K}$. The difficulty to achieve a single magnetic domain is manifested in a severe overlap between diffraction peaks and in consequence the direction of the magnetic moment in the cell cannot be determined unambiguously.

As mentioned before, SrRuO₃ has been studied theoretically by means of a multitude of methods. The main reason is that in spite of the 4d-magnetism, the compound has been considered to exhibit strong electron-electron correlations. Recently it has been suggested

(both by experiment^{43,44} and theory⁴⁵) that the electronic correlations in SrRuO₃ are weak. In the following we wish to provide an extensive analysis of the properties of this compound and, by comparing the calculated results to experimental data, make an assessment on the degree of electron correlations and the best suited method to treat the electronic structure of SrRuO₃ and related ruthenates.

A. Volume trends

Due to the fact that the phase diagram of SrRuO₃ is not a simple one, it is far from sufficient to compare calculated values of magnetic moments with the measured values, without making a careful analysis regarding the volume dependence of the moments. In the following we will show that there is quite a strong volume dependence of the magnetic moments. This might in fact be one of the reasons for the wide range of calculated magnetic moments, available in the literature.

We start by determining the equilibrium volume for SrRuO₃ in both the orthorhombic as well as the cubic phase. The calculated equilibrium volumes (V_{eq}^{calc}) determined within DFT and different approximations for the exchange-correlation as well as Hubbard-corrected LDA functionals and LDA+DMFT are summarised and compared to experimental data^{8,42} in Fig. 1 and Table I.

We have performed calculations for a range of volumes (for both orthorhombic and cubic phases), using the methodologies mentioned above. We fit the results to the universal equation of state by Vinet et al.⁴⁶ and from this we extract the equilibrium volume and bulk modulus (Tab. I). The calculated volumes and bulk modulus are compared to experimental values for the orthorhombic phase. The experimental bulk modulus B_0 is ≈ 192 GPa, from Ref. 47. The experimental volume is ≈ 408.6 a.u.³ according to Bushmeleva et al.⁴² and ≈ 406.5 a.u.³ as estimated by Kanbayashi⁸.

We begin by examining the volumes for the orthorhombic structure given by the different methods. The calculated equilibrium volume is similar for all three LDA functionals, only a slight over binding is seen for this compound (around 1.6%-2%), while LDA+DMFT provides slightly better results (only a 1.5% underestimation relative to the experimental volume). There is a prominent difference between the equilibrium volumes calculated with the LDA (PW91, PZ81, vBH72) and GGA (PBE96) functionals. Typically an LDA treatment results in over binding, while GGA in under binding and an overestimation of the ground state volume. As expected the PBE96 functional under binds also for SrRuO₃, resulting in a 6% larger volume than the experimental value. On the other hand, the AM05 functional is in better agreement with the experimental volume with only about 1% under binding. With the exception of PBE96, which leads to a strong overestimation of the volume, all other functionals considered in this study reproduce rather well the exper-

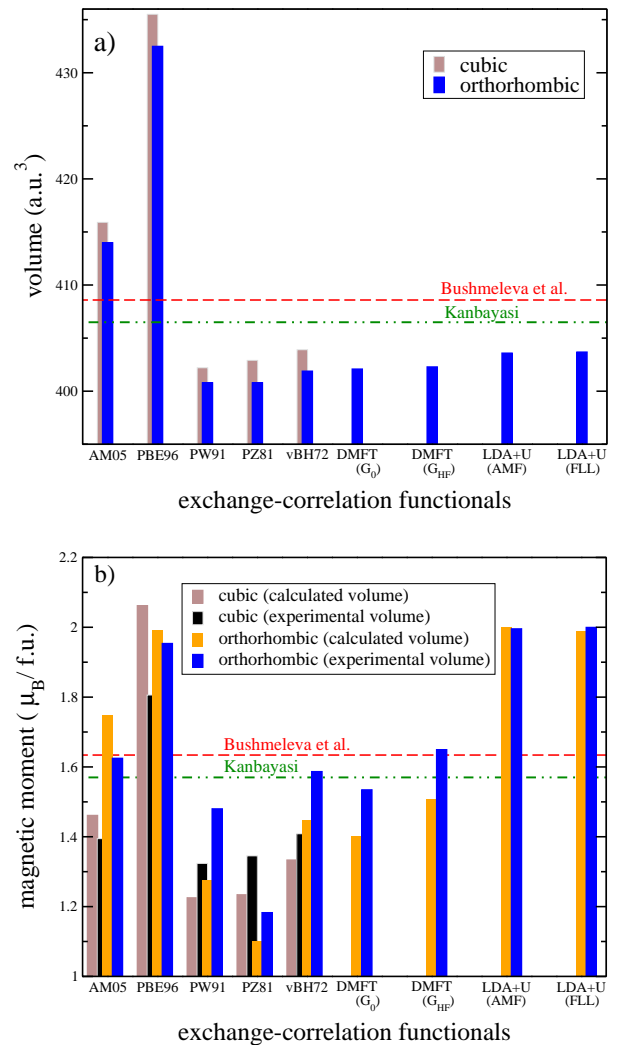


FIG. 1. (colour online) (a) Calculated equilibrium volumes (V_{eq}^{calc}) determined by different methods and functionals (LDA, GGA, LDA+DMFT, LDA+U with $U=3.0$ eV). (b) Spin magnetic moments per formula unit calculated for both the experimental volume⁴² as well as for the calculated equilibrium volumes. Both cubic (brown and black bars) and orthorhombic (blue and orange bars) structures have been considered. The experimentally determined values for saturation volume for single crystal bulk samples (Fig. 1a) and their corresponding magnetic moments (Fig. 1b) are marked by red dashed lines⁴² and green dash-dotted lines⁸.

imental volume. Regarding the bulk modulus, the experimental values are in good agreement with the calculated values for all the functionals used with the exception of PBE96 and AM05 (see Table I).

In order to estimate the effect of the octahedral tiltings and rotations on the properties of this compound, we have also considered the cubic phase of SrRuO₃ and calculated the equilibrium volume and bulk modulus using different methods (Tab. I and Fig. 1). The differences in bulk modulus and equilibrium volumes between the cu-

Orthorhombic structure				
E_{xc}	$\langle gS \rangle$ /f.u. experim. vol.	V_0 [a.u. ³]	$\langle gS \rangle$ /f.u. calc. vol.	B_0 [GPa]
AM05	1.625 μ_B	413.957	1.749 μ_B	178.2
PBE96	1.954 μ_B	432.465	1.993 μ_B	161.9
PW91	1.481 μ_B	400.794	1.275 μ_B	201.9
PZ81	1.183 μ_B	400.798	1.100 μ_B	202.3
vBH72	1.587 μ_B	401.909	1.447 μ_B	200.8
DMFT(G_0)	1.535 μ_B	402.124	1.403 μ_B	188.8
DMFT(G_{HF})	1.649 μ_B	402.317	1.509 μ_B	185.0
LDA+ U (AMF)	1.996 μ_B	403.555	1.989 μ_B	201.2
LDA+ U (FLL)	2.000 μ_B	403.669	2.000 μ_B	202.6
experimental ⁴²	1.634	408.6	-	192.0
Cubic structure				
AM05	1.395 μ_B	415.9	1.462 μ_B	172.7
PBE96	1.806 μ_B	435.5	2.062 μ_B	152.0
PW91	1.324 μ_B	402.2	1.226 μ_B	191.3
PZ81	1.345 μ_B	402.9	1.234 μ_B	198.9
vBH72	1.334 μ_B	403.9	1.409 μ_B	196.6

TABLE I. Magnetic moment per formula unit calculated with different methods, for the orthorhombic and cubic phases of SrRuO₃. For the LDA+ U and LDA+DMFT calculations a $U = 3$ eV was used.

bic and orthorhombic phases illustrates the importance of the octahedral distortions for the cohesive properties of SrRuO₃.

B. Calculated spin moments

In the following we investigate the change in magnetic moment induced by changes in volume and structural properties, see Fig. 2 for details. It should be mentioned that we deal with *isobaric* volume changes, meaning that the a to b to c ratio has been conserved for all calculations.

In order to account for possible basis-set dependence of the calculated values, we have also investigated how the trend in volume changes as a function of the chosen basis set, i.e. the difference between a triple- κ basis and a double κ -basis. We find that for the equilibrium volume the differences are minute, $\approx 0.1\%$ for the cubic structure and $\approx 10^{-3}\%$ for the orthorhombic structure for both LDA (vBH72) and GGA (AM05). For the magnetic moment at the experimental volume we find that the cubic phase is insensitive to whether we use a double- or triple- κ basis set, with difference of $\approx 0.5\%$ for both LDA and GGA. The orthorhombic structure is more sensitive, with a $\approx 5\%$ difference in moment, highlighting the importance of a good basis set in the interstitial region to describe the effects of the octahedral distortions.

We highlight the variations of the magnetic properties of SrRuO₃ due to different treatments of the exchange correlation within DFT as well as DFT+DMFT (see Tab. I and Fig. 2). These differences are much larger than what one normally finds in other compounds. In the or-

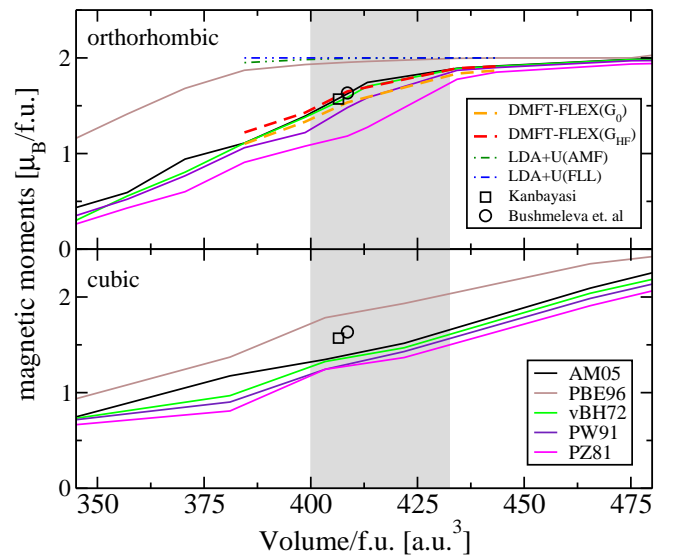


FIG. 2. (colour online) Magnetic moment variations induced by changes in volume for both the orthorhombic (upper panel) and the cubic (lower panel) phases. For each chosen value of the volume, the moments have been calculated with different LDA/GGA functionals, LDA+DMFT and LDA+ U , with $U = 3.0$ eV. The shaded area marks the range of values for the calculated equilibrium volumes. Experimental data-points for saturation moment for single crystal bulk samples of the orthorhombic phase are included, originating from Refs. 8 (square) and 42 (circle).

thorhombic structure, the delicate nature of the magnetic moment is evident, the parametrization by von Barth and Hedin results in a moment almost 30% larger than that of the parametrization by Perdew and Zunger. Note also that the magnetic moment obtained with PBE96 is already in the higher end of the scale at the experimental volume, and even becomes larger at the calculated equilibrium volume.

For the orthorhombic structure, the most accurate predictions of the magnetic moments for the experimental volumes have been provided by the LDA+DMFT-SPTF (G_{HF}), by the LDA (vBH72) and the GGA functional, AM05. The LDA+ U , for both double counting corrections (AMF and FLL), as well as the PBE96 provide an overestimated magnetic moment for the entire volume range considered, while providing a very robust magnetic moment with respect to volume changes for almost the entire range considered. The LDA+DMFT-SPTF (G_0) only slightly underestimates the value of the moment (Fig 2). When varying the volume, the changes in the magnetic moment follow the same trend (with less than 7% difference in values) when treated with LDA+DMFT-SPTF (G_0) or LDA+DMFT-SPTF (G_{HF}). The volume (for both orthorhombic and cubic phases) has been varied well below and above the calculated equilibrium values, in order to offer a complete picture of the magnetic moments' sensitivity to *isobaric* volume changes. In the

orthorhombic structure, at volumes larger than V_{eq}^{calc} , the calculated magnetic moments converge to the same value independently of the methods used, while for volumes smaller than V_{eq}^{calc} the magnetic moments are much more sensitive to the different methods employed. The gray shaded area in Fig. 2 marks the range of calculated (with different methods) equilibrium volumes. Within this range (that encompasses 35 a.u.³ around the experimental volume) for a volume compression of 8% the decrease registered in the magnetic moments vary from $\approx 20\%$ for LDA+DMFT and vBH72 to almost 40% for PZ81.

The magnetic moment as a function of volume shows similar trends for all the functionals, as long as we are far from a half-metallic state, the key issue lies in the displacement of the curves. However PBE96 localizes the electrons too much (discussed in details below) and this produces a magnetic moment that is insensitive to volume changes around the experimental volume. Gu et al.⁴⁸ reports on the change in moment for a SrRuO₃ film relaxed on a SrTiO₃ substrate, showing that a strain of 1% gives a change in moment of the order of $0.1\mu_B$. The relaxation procedure is however not volume conserving and volume changes might be partly responsible for this. Around the experimental volume, both LDA+DMFT method, with SPTF in G_0 and G_{HF} , show the same behaviour of magnetic moments with changes in volume. Fig. 2 shows that one should be careful when comparing calculated magnetic moments, because they can differ strongly with respect to the considered volume and the method used. The experimental situation is such that the strong moment anisotropy makes it difficult to achieve saturation moments for polycrystalline samples. However, a few single crystal results have been reported (e.g. Ref. 8, 49, and 50). As suggested in Ref. 13, on-site correlations to the Ru 4d states improve the description of the electronic structure. In general, smaller changes in the description of the electronic structure, as given by different parametrizations of LDA, can cause (after the self-consistent cycle is done) variations in the calculated magnetic moment.

With regard to this quantity the AM05 functional performs excellently. The LDA+U method creates a too strong localization of the d -electrons (discussed below), and the magnetic moment overshoots the experimental one. The equilibrium volume also increases with U , an effect of the decreased contribution to bonding by the increasingly localized d -states. The LDA+DMFT method includes dynamic screening, reducing the tendency of localisation. In addition, this method increases the electron effective mass. For the chosen value of U the magnetic properties of SrRuO₃ are very well reproduced by theory (see Fig. 2).

C. Effects of on-site Coulomb interaction

Due to the delicate nature of the electronic structure of SrRuO₃, it becomes of interest to investigate how the strength of the electron correlations influences the electronic structure and magnetic properties of this material. We therefore inspect the evolution of the magnetic moment when changing the strength of the on-site Coulomb interaction, in both the cubic and orthorhombic phases (Fig. 3). Using LDA+U with AMF double-counting correction the moment of the orthorhombic phase increases monotonically from the von Barth-Hedin LDA value of $1.6\mu_B$ towards $2\mu_B$ (see Fig. 3). This means that we quickly reach (already for $U=2$ eV) a higher moment than the highest reported experimental one. The high moment solution, characterised by an integer moment of $2\mu_B$, is due to the fact that the electronic structure becomes half-metallic, which we will notice in the density of states below. Also, a further analysis in connection to the LDA+U (FLL double-counting correction) calculation results in a higher moment with increasing values of U . When we consider SrRuO₃ in the cubic structure, the moment reaches it's maximum for $U=2$ eV, approaching the (AMF) solution at $U=4$ eV. For the orthorhombic phase, there are only very small differences between the values obtained by employing the different double counting corrections on LDA+U. In the cubic phase the differences are bigger.

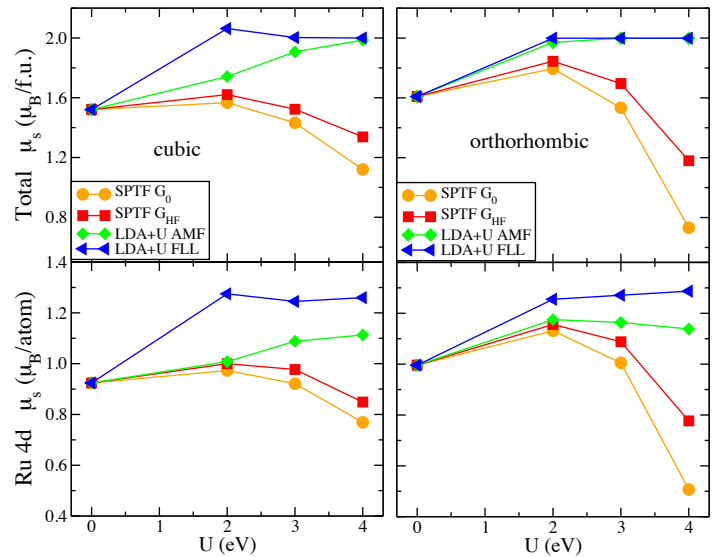


FIG. 3. (colour online) Calculated total magnetic moments and the Ru 4d moments, for both cubic and orthorhombic phases, as a function of the Hubbard U , when using the solvers SPTF(G_0) and SPTF(G_{HF}) within LDA+DMFT and different double-counting corrections (AMF and FLL) within LDA+U.

As the electrons in SrRuO₃ also have an itinerant character, it is a good idea to use a method that allows

for dynamic screening of the coulomb interaction, such as LDA+DMFT. The LDA+DMFT calculation with the SPTF(G_0) solver results in an initial slight increase, followed by a strong reduction of the magnetic moment when U increases, for both the cubic phase as well as the orthorhombic one. In the cubic phase the moment is always lower or equal to the LDA value, for all values of U considered. Electron correlations, i.e. effects beyond Hartree-Fock theory, are often argued to cause a reduction in the exchange splitting, and hence a lowered magnetic moment. The cubic phase of SrRuO₃ seems to follow this rule. For the orthorhombic phase the scenario is a little bit more complex, since initially there is an increase in the moment with increasing U , after which a strong decrease is found (Fig. 3). Calculations based on SPTF(G_{HF}) and SPTF(G_0) give similar results, although when treated within SPTF(G_{HF}) the moment is not reduced as strongly, with increasing U .

In order to get a deeper insight into the electronic structure of SrRuO₃, we investigate the sensitivity of the effective mass to the considered on-site Coulomb interactions. The only method in this study capable of capturing a renormalised quasiparticle weight Z is LDA+DMFT. The experimental mass enhancement arises both from electron-electron interaction as well as electron-boson interactions, as recently suggested by Shai et al.⁴¹. The latter can be electron-phonon or electron-magnon interactions. We calculate the spin resolved contribution from the electron-electron interaction only. For both the cubic and orthorhombic phases, the dependence on the Hubbard U of the spin resolved quasiparticle weight values are depicted in Fig. 4.

Experimental data for the effective mass (inverse of Z) are rather abundant. EELS data by Cox et. al¹⁸ show an effective mass of about $\frac{m^*}{m_0} \approx 3.6$, this relies on the assumption that only one free electron is available per Ru atom. On the other hand, angular resolved de Haas van Alphen data indicate at least seven bands crossing the Fermi level, with an effective mass ratio of $4.1 \leq \frac{m^*}{m_0} \leq 6.9$ ⁵¹. Specific heat measurements show $\frac{m^*}{m_0} \approx 3.0 - 3.1$ ^{19,20}, while older experiments by Allen et.al⁵² and Okamoto et.al⁵³ provide a value closer to 4.43. This leads to a quasiparticle weight in the vicinity of $0.15 < Z < 0.35$. We draw the attention of the reader to the fact that the experimental values corresponding to the mass enhancements that we mentioned above, have been extracted by different methods from the raw experimental data. In some cases even values calculated from first principles have been used in the fitting equations. To some extent, these values might depend on the way they have been extracted from the measured spectra.

We consider the EELS and specific heat measurements to be most representative when comparing to a band-integrated quasiparticle weight. The results using SPTF(G_0) for $U = 4\text{eV}$ compare well with the experimental number, with $Z \approx 0.4$, considering the quenching of the magnetic moment this is however not representa-

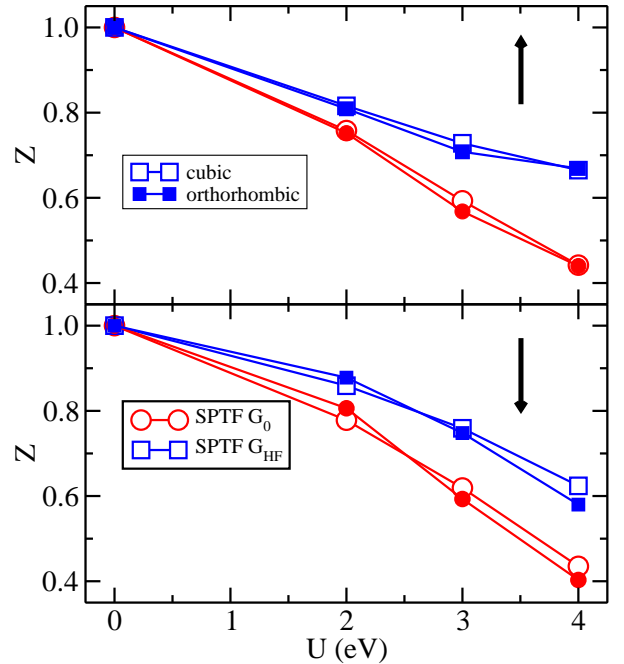


FIG. 4. (colour online) Dependence of the calculated quasi particle weight Z on the Hubbard U and the different LDA+DMFT solvers SPTF(G_0) (circles) and SPTF(G_{HF}) (squares). The filled symbols represent the orthorhombic phase, while the empty symbols represent the cubic phase. The two panels give spin resolved information.

tive for the compound. An estimate of $Z \approx 0.55$ for the electronic part of the mass enhancement, as for $U = 3\text{eV}$ is more reasonable. SPTF(G_{HF}) results in a slightly higher $Z \approx 0.7$, that should be a better estimate than SPTF(G_0) due to the under screening of the Coulomb interaction in the latter. Recent ARPES spectra by Shai et al.⁴¹ reveals a kink in the spectra close to the Fermi level, a text-book example of electron-boson coupling, most likely magnons. Hence this contribution will not show up in the single site LDA+DMFT approach. We estimate the local electronic correlation to give a contribution of $0.5 < Z < 0.7$, and attribute the remaining part to electron-boson coupling. One further possible reason for the remaining difference between theory and experiments could be that the inclusion of spin-orbit coupling has a large impact on the weights; it has previously been shown to be important for the Fermi surface geometry of the related compound Sr₂RhO₄⁵⁴. However, we find only a small difference in the calculated quasiparticle weights, with and without the inclusion of spin-orbit coupling effects, amounting to 0.76%.

D. Spectral properties

There are two experimental studies of the valence band spectrum of orthorhombic SrRuO₃ that we are aware of. One is by D. Toyota et al.⁵⁰ and represents an investigation of a single crystal film, with a thickness up to 100 ML. The other study has been performed on a polycrystalline bulk sample⁵³. We chose to compare our calculations to the single crystal data, which are expected to better represent a calculation which does not consider effects of grain boundaries.

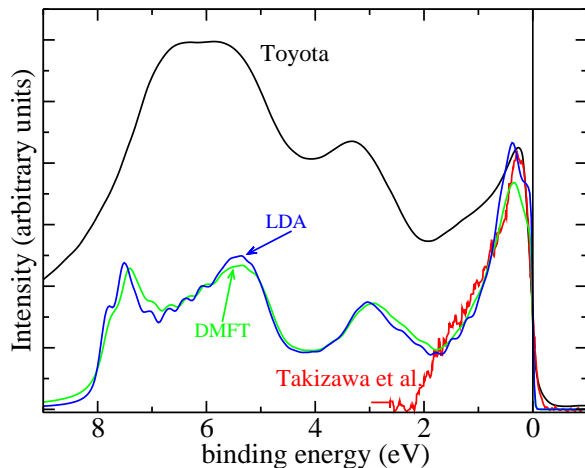


FIG. 5. (colour online) Photoemission spectra of bulk SrRuO₃⁴⁹ (red line) and 100ML thick SrRuO₃ films⁵⁰ (black line) compared to calculated spectra obtained within LDA (blue line) and LDA+DMFT, SPTF- G_{HF} with $U=2\text{eV}$ (green line). Both PES were taken at 600 eV. Note that the intensity is given in arbitrary units for both theory and experiment. The theoretical spectra is calculated by summing the products of the l -projected DOS with the l -projected cross sections for the photoelectron excitation with photons of 600 eV energy from Ref. 55. No additional broadening of the theoretical spectra is added.

The photoemission data by Toyota et al. for 100ML SrRuO₃, shows three very clear peaks (Fig. 5 shows this experimental spectrum). The highest peak is located 0.3-0.5 eV below the Fermi level. In addition there is one level found at approximately $E_F - 3.5$ eV and a larger, broader feature between 4 and 8 eV below the Fermi level. These two lower-most peaks are mainly composed of oxygen 2*p*-states, though the lowest lying peak has a considerable amount of Ru 4*d*-character. The peak close to the Fermi level is almost entirely of Ru 4*d* character, and is therefore most suitable to compare with and to determine the quality of our calculated spectral functions, shown in Fig. 5 and 6. The LDA+ U result, displayed in Fig. 6 show a half-metallic state for

$U > 3$ eV similar to what Jeng et al.¹⁵ obtained. This is not consistent with experimental findings⁴². Both LDA and LDA+DMFT provide metallic states in both spin channels. In fact the LDA and the LDA+DMFT spectra are surprisingly similar. The top most peak shows some renormalization and is pushed closer to the Fermi level in the LDA+DMFT scheme. Comparing to previously published spectral functions with similar methodology we see an overall agreement¹⁴. Both LDA and LDA+DMFT methodologies show good agreement with experimental photo-emission data. In Fig 5 we compare our theoretical curves (LDA and LDA+DMFT results) to experimental data of Toyota et al. and Takizawa et al.^{49,50}. The theoretical spectra are calculated by summing the products of the l -projected DOS with the l -projected cross sections for the photoelectron excitation with photons of 600 eV energy from Ref. 55. In the 0-2 eV binding energy regime, both experiments as well as both theoretical curves are similar. A peak appearing around 3 eV binding energy is well reproduced by theory, it is mainly of oxygen character with some Ru 4*d* hybridisation. In the experiments by Toyota et al. a large feature of hybridising O 2*p* and Ru 4*d* states is found between 5 and 8 eV binding energy, also this is well captured by theory, although slightly broader. The relative intensities of all peaks are in good agreement with the experimental spectra.

E. Effects of spin-orbit coupling

Spin-orbit interaction introduces a coupling between spin space and real-space, giving rise to a number of interesting phenomena. For example the magneto-crystalline anisotropy (MCA) which is important from a technological perspective, as it dictates the ability of the moment to remain in the same direction under an external field. SrRuO₃ is regarded to have a very strong MCA for being a transition metal compound. It is also argued to have a universal MCA, i.e. the easy axis is always aligned to the strain field⁵⁶.

Grutter et al.⁵⁶ determined the orbital moments for thick films to be in the order of $0.06\mu_B$. Strained films reach much higher orbital moments as the crystal field splitting is further reduced, up to $0.3\mu_B$ is reported⁵⁶. The calculated orbital moments, obtained here, for the bulk orthorhombic structure at the equilibrium volume is around $0.01\mu_B$ for all functionals, i.e. lower than the reported experimental value.

More interestingly, the orbital moment is not collinear with respect to the spin moment for the orthorhombic structure. This severely complicates measurements of magneto-optical properties⁵⁷, and XMCD measurements of orbital moments, as the sum-rules are expressed in terms of the z -components of the spin and orbital moments⁵⁸. Experimental measurements of the tilted orbital moments might be possible using EMCD⁵⁹, where atomic resolution might be accomplished using electron

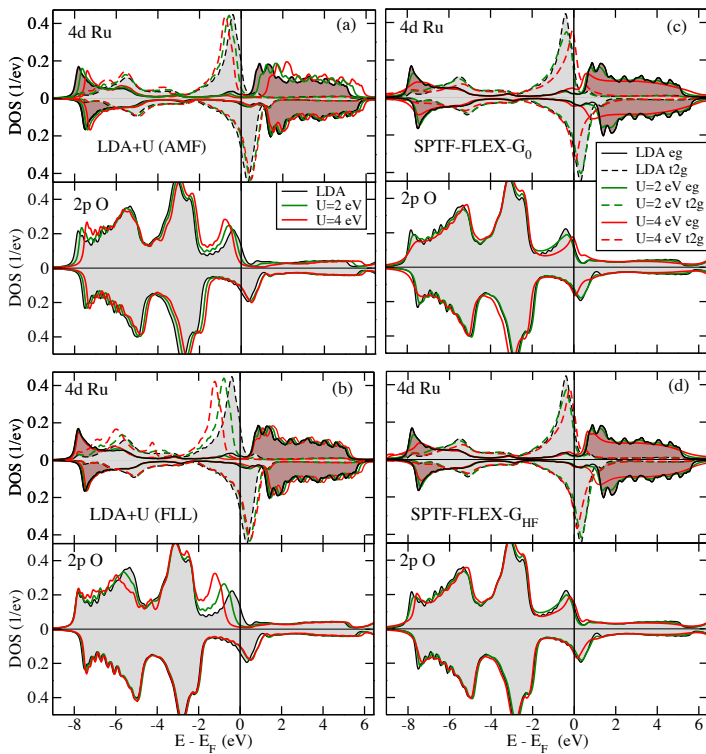


FIG. 6. (colour online) Calculated DOS for SrRuO₃ in the orthorhombic structure. Left-panel: LDA and LDA+U results with different double counting corrections: (a) around mean field (AMF) and (b) fully localized limit (FLL). Right-panel: calculated DOS within LDA+DMFT with two different solvers, (c) SPTF-FLEX G₀ and (d) SPTF-FLEX G_{HF}.

vortex beams⁶⁰.

The non-collinear ordering of spin and orbital moments in distorted perovskites is intrinsically coupled to the tiltings and rotations of the oxygen octahedra, as previously noted by Refs 61 and 62. When an external magnetic field is used to rotate the magnetic moments away from the easy axis, it is known that the non-collinear ordering between the spin and orbital moments appears.

In surface geometries where we have a strong out of plane MCA, it is known that the presence of an in-plane magnetic field, aligning the spin-moment in the plane, results in a non-collinear ordering of spin and orbital moments. In these geometries the strong MCA will try to rotate the orbital moments towards the spin moment, a strong crystal field counteracts the alignment to the spins, and induce an orbital moment component along the easy axis⁶³. Thus, the spin and orbital moments may not always be aligned.

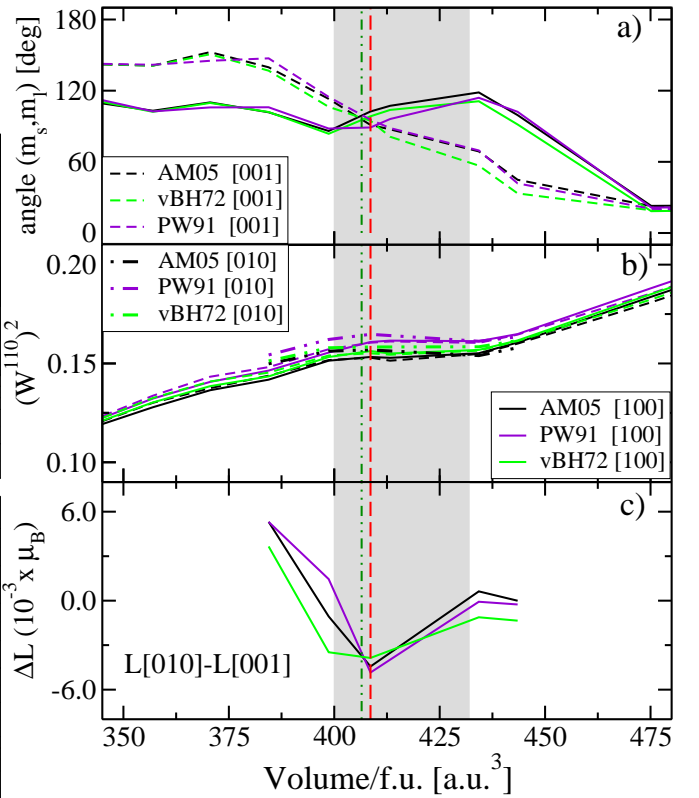


FIG. 7. (colour online) a) Volume dependence of the angle between spin moment to orbital moment b) square of the w^{110} tensor component, proportional to the isotropic spin-orbit coupling. The experimental volumes values are marked by vertical lines: red dashed lines⁴² and green dash-dotted lines⁸. The gray shaded area marks the region of the calculated equilibrium volumes. The angles between the spin and orbital moments have been calculated along two different crystallographic directions: [001] (solid lines) and [010] (dashed lines). In (c) the orbital moment anisotropy (OMA) is shown.

In distorted perovskites this picture becomes more complicated. The strong exchange coupling drives the spin moments to be in principle collinear⁶⁴, but the rotated oxygen octahedra results in crystal fields that induce orbital components in other directions. The orbital moment components aligned orthogonal to the spin moment are antiferromagnetically aligned with respect to each other, whereas the parallel component is ferromagnetically aligned. The ordering type is presented in Tab. II for all considered functionals, including the LDA+U and LDA+DMFT calculations.

The ordering of the different components of the orbital moment is completely insensitive to the choice of the exchange-correlation functional and additional treatment of correlation in terms of LDA+U and LDA+DMFT (in both approaches one has to take care that a rotationally invariant description of the Coulomb interaction is used).

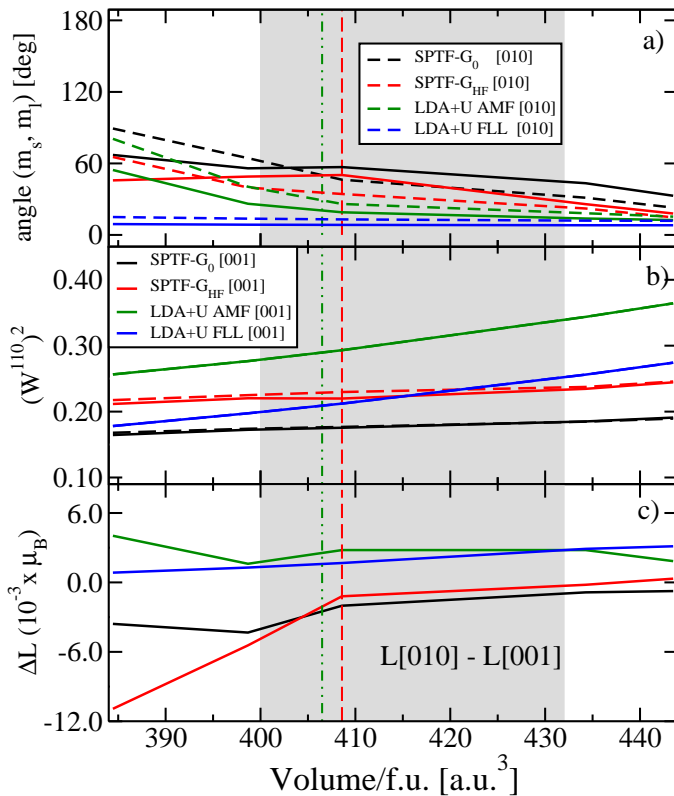


FIG. 8. (colour online) Volume dependence of (a) the angle of the spin moment with respect to the orbital moment (b) square of the w^{110} tensor component (proportional to the isotropic spin-orbit coupling) and (c) the orbital moment anisotropy. The represented quantities have been calculated within different approaches: SPTF-FLEX- G_0 , SPTF-FLEX- G_{HF} , LDA+U (AMF and FLL). The angles between the spin and orbital moments (a) have been calculated along two different crystallographic directions: [001] (solid lines) and [010] (dashed lines). The experimental volume values are marked by vertical lines: red dashed lines⁴² and green dash-dotted lines⁸. The gray shaded area marks the region of the calculated equilibrium volumes.

It is also insensitive to volume changes and is a direct effect of the distortions of the oxygen octahedra, since the tilting and rotation angles are taken from experimental data only the strength of the crystal field and hybridisation will change with changing volume. As Tab. II shows, volume changes under such conditions do not affect the type of ordering but the magnitude of the components of the orbital moment do change. This causes the angle between spin and orbital moment to have a volume dependence even without changes in the tilting and rotation angles of the oxygen octahedra.

The magnitude of each component of the orbital moment is controlled by the strength of the crystal field and hybridisation. The hybridisation changes significantly between different treatments of exchange-correlation,

Spin alignment	Ordering of orbital components		
	m_x	m_y	m_z
[010]	AFM C-type	Ferromagnetic	AFM G-type
[001]	AFM A-type	AFM G-type	Ferromagnetic

TABLE II. The table shows the ordering between the x -, y - and z - components of the orbital moments in the four different Ru octahedra for the spin aligned along the easy [010] axis or [001] hard axis. This ordering is the same for all methods tested, including LDA+U and LDA+DMFT, and is robust with respect to changes in volume.

hence the angle between the spin and orbital moments is an extremely sensitive probe for differences in the theoretical treatment. Investigating this we see a clear trend, when treating the system within LDA/GGA (Fig. 7) and within LDA+U/DMFT (Fig. 8). When the electrons in SrRuO₃ are treated within LDA/GGA, the angles between the spin and orbital moments at the experimental volume have almost the same values (≈ 90 - 100°), independent of the spin direction ([010] or [001]) along which they were estimated. For increasing volume, the moments go from being mostly anti-parallel as dictated by Hund's third rule, to being mostly parallel, as can be seen in panel a) of Fig. 7. When SrRuO₃ is treated within LDA+U and LDA+DMFT, the angles between moments exhibit almost the same trend for both [001] and [010] spin directions, for the whole range of considered volumes. Independent of the functionals used for treating the electronic system, for very large volumes the spin and orbital moments tend to align parallel to each other, see panel a) of Fig. 8). At the experimental volume, the angles determined within LDA+U and LDA+DMFT show a stronger variation than when treated with LDA/GGA functionals, leading to variations in direction from 8° to 57° . The magnitude of the angles is also here determined by the interplay between the crystal fields and the hybridisation, it is evident that the different treatments of exchange and correlation on the Ru 4d-shell impacts the hybridisation significantly. The impact of the spin-orbit coupling on the energetics can be estimated by calculating the expectation value of $l \cdot s$. Using the tensor moment formalism⁶⁵ the isotropic spin-orbit coupling is equivalent to the $w^{110} = (ls)^{-2} \sum_i \vec{l}_i \cdot \vec{s}_i$ tensor. This is plotted in panel b) of Fig. 7 and 8 as a function of volume. One can see a clear increase in the role of the spin-orbit coupling on the energetics as the volume increases. This indicates the dominance of the kinetic hybridization/crystal field effects for smaller volumes. Close to the experimental volume the angles are quite similar for both the [010] and the [001] spin directions.

For conventional monoatomic solids the MCA is proportional to the anisotropy of the orbital moment⁶⁶. Due to the non-trivial angle between the spin and orbital moment and the polyatomic nature of the compound this is not expected to hold for SrRuO₃. The orbital magnetic anisotropy presented here isolates effects from changes in

volume, as the tilting and rotation angles are kept fixed. The OMA is expected to change, as well as the MCA, when lattice relaxations are taken into account. Uniaxial strain, as occurring in thin films, is expected to give a very large contribution as the oxygen octahedra will be elongated/compressed in the direction of the strain, resulting in a more anisotropic environment for the Ru-ion.

As mentioned above, we have estimated the spin-orbit coupling influence on the mass enhancement to be negligible.

IV. CONCLUSIONS

We have investigated the electronic structure, cohesion and magnetism of SrRuO₃, both in the high temperature cubic phase as well as in the low temperature orthorhombic phase. Several parametrizations of the LDA and GGA functionals were used, as well as the LDA+U method and LDA+DMFT in combination with a FLEX solver. We find that LDA, LDA+U, AM05 and LDA+DMFT reproduce the equilibrium volume and bulk modulus with reasonable accuracy, whereas the GGA functional PBE96 seems to be less accurate. When it comes to the magnetism, LDA, AM05 and LDA+DMFT reproduce the delicate spin moments of the orthorhombic structure with good accuracy, whereas LDA+U and PBE96 overestimate the spin moments significantly. Taking all this information into account, we conclude that LDA, AM05 and LDA+DMFT reproduce the ground state properties of SrRuO₃ very well. In addition to this, LDA+DMFT provides information about the mass enhancement due to local electronic correlation. This points to that SrRuO₃ is a weakly correlated metal, for which

the effective mass is enhanced significantly compared to that given by single particle theory. The LDA+U results are found to localize the 4d states of the Ru atom too strongly, in line with the experience with self-interaction corrected theories⁴⁵. We also find that the calculated spin moments are quite sensitive to the equilibrium volume, a result which should be possible to verify experimentally. We show furthermore that the coupling between spin and orbital moments is highly non-collinear, with angles ranging from 0 to 150 degrees, depending on the level of accuracy for the exchange correlation functional and the volume considered for the calculation. An experimental verification of this behaviour would be highly interesting, although challenging due to the symmetry of the orthorhombic crystal structure. Regarding the electronic structure we find that both LDA, AM05 and LDA+DMFT reproduce the measured valence band spectrum with good accuracy. Therefore, in conclusion, we recommend the GGA (AM05) or LDA+DMFT for further investigations on SrRuO₃ regarding the properties considered here.

ACKNOWLEDGMENTS

The support from the Swedish Research Council (VR) is thankfully acknowledged. O.G. is thankful for support by the eSSSENCE network for funding time to improve implementations that allowed for this study. O.E. acknowledges support from the KAW foundation and the ERC (Grant No. 247062-ASD). The computer calculations have been performed at the Swedish high performance centres HPC2N, NSC and UPPMAX under grants provided by the Swedish National Infrastructure for Computing (SNIC).

-
- ¹ J. Lee, M. P. Allan, M. A. Wang, J. Farrell, S. A. Grigera, F. Baumberger, J. C. Davis, and A. P. Mackenzie, *Nat Phys* **5**, 800 (2009).
- ² Y. Maeno, H. Hashimoto, K. Yoshida, S. Nishizaki, T. Fujita, J. G. Bednorz, and F. Lichtenberg, *Nature* **372**, 532 (1994).
- ³ J. Mravlje, M. Aichhorn, T. Miyake, K. Haule, G. Kotliar, and A. Georges, *Phys Rev Lett* **106**, 096401 (2011).
- ⁴ L. Klein, L. Antognazza, T. Geballe, M. Beasley, and A. Kapitulnik, *Phys Rev B* **60**, 1448 (1999).
- ⁵ R. V. K. Mangalam and A. Sundaresan, *Materials Research Bulletin* **44**, 576 (2009).
- ⁶ I. Mazin and D. Singh, *Phys Rev B* **56**, 2556 (1997).
- ⁷ B. Dabrowski, O. Chmaissem, P. Klamut, S. Kolesnik, M. Maxwell, J. Mais, Y. Ito, B. Armstrong, J. Jorgensen, and S. Short, *Phys Rev B* **70**, 014423 (2004).
- ⁸ A. Kanbayasi, *J Phys Soc Jpn* **41**, 1876 (1976).
- ⁹ G. Koster, L. Klein, W. Siemons, G. Rijnders, J. Dodge, C.-B. Eom, D. Blank, and M. Beasley, *Rev Mod Phys* **84**, 253 (2012).
- ¹⁰ M. Ziese, I. Vrejoiu, E. Pippel, P. Esquinazi, D. Hesse, C. Etz, J. Henk, A. Ernst, I. V. Maznichenko, W. Hergert, et al., *Phys Rev Lett* **104**, 167203 (2010).
- ¹¹ Z. Fang, N. Nagaosa, K. Takahashi, and A. Asamitsu, *Science* **302**, 92 (2003).
- ¹² I. Felner, K. Nomura, and I. Nowik, *Phys Rev B* **73** (2006).
- ¹³ J. Rondinelli, N. Caffrey, S. Sanvito, and N. Spaldin, *Phys Rev B* **78**, 155107 (2008).
- ¹⁴ E. Jakobi, S. Kanungo, S. Sarkar, S. Schmitt, and T. Saha-Dasgupta, *Phys Rev B* **83**, 041103 (2011).
- ¹⁵ H.-T. Jeng, S.-H. Lin, and C.-S. Hsue, *Phys Rev Lett* **97**, 067002 (2006).
- ¹⁶ H. Hadipour and M. Akhavan, *Eur Phys J B* **84**, 203 (2011).
- ¹⁷ P. Kostic, Y. Okada, N. Collins, Z. Schlesinger, J. Reiner, L. Klein, A. Kapitulnik, T. Geballe, and M. Beasley, *Phys Rev Lett* **81**, 2498 (1998).
- ¹⁸ P. Cox, R. Egdell, J. Goodenough, A. Hamnett, and C. Naish, *J Phys C Solid State* **16**, 6221 (1983).
- ¹⁹ G. Cao, S. McCall, M. Shepard, J. Crow, and R. Guertin, *Phys Rev B* **56**, 321 (1997).
- ²⁰ J. Ahn, J. Bak, H. Choi, T. Noh, J. Han, Y. Bang, J. Cho, and Q. Jia, *Phys Rev Lett* **82**, 5321 (1999).

- ²¹ L. de' Medici, J. Mravlje, and A. Georges, *Phys Rev Lett* **107**, 256401 (2011).
- ²² A. Georges, L. d. Medici, and J. Mravlje, *Annu Rev Condens Matter Phys* **4**, 137 (2013).
- ²³ D. Vollhardt, *Annalen der Physik* **524**, 1 (2011).
- ²⁴ G. Kotliar, S. Y. Savrasov, K. Haule, V. S. Oudovenko, O. Parcollet, and C. A. Marianetti, *Rev Mod Phys* **78**, 865 (2006).
- ²⁵ J. M. Wills, M. Alouani, P. Andersson, A. Delin, O. Eriksson, and O. Grechnev, *Springer Series in Solid-State Sciences* pp. 1–195 (2010).
- ²⁶ A. Grechnev, I. Di Marco, M. I. Katsnelson, A. I. Lichtenstein, J. Wills, and O. Eriksson, *Phys Rev B* **76**, 035107 (2007).
- ²⁷ O. Grånäs, I. Di Marco, P. Thunström, L. Nordström, O. Eriksson, T. Björkman, and J. M. Wills, *Computational Materials Science* **55**, 295 (2012).
- ²⁸ <http://www.fplmto-rspt.org/>.
- ²⁹ J. M. Wills and B. R. Cooper, *Phys Rev B* **36**, 3809 (1987).
- ³⁰ P. E. Blochl, O. Jepsen, and O. Andersen, *Phys Rev B* **49**, 16223 (1994).
- ³¹ U. Barth and L. Hedin, *J Phys C Solid State* **5**, 1629 (1972).
- ³² J. Perdew and Y. Wang, *Phys Rev B* **45**, 13244 (1992).
- ³³ J. Perdew and A. Zunger, *Phys Rev B* **23**, 5048 (1981).
- ³⁴ R. Armiento and A. Mattsson, *Phys Rev B* **72**, 085108 (2005).
- ³⁵ J. Perdew, K. Burke, and M. Ernzerhof, *Phys Rev Lett* **77**, 3865 (1996).
- ³⁶ L. Pourovskii, M. Katsnelson, and A. Lichtenstein, *Phys Rev B* **72**, 115106 (2005).
- ³⁷ O. Grånäs, Ph.D. thesis, Uppsala University, *Materials Theory* (2012).
- ³⁸ N. Bickers, D. Scalapino, and S. White, *Phys Rev Lett* **62**, 961 (1989).
- ³⁹ A. Lichtenstein, M. Katsnelson, and G. Kotliar, *Phys Rev Lett* **87**, 067205 (2001).
- ⁴⁰ E. Şaşoğlu, C. Friedrich, and S. Blügel, *Phys Rev B* **83**, 121101 (2011).
- ⁴¹ D. E. Shai, C. Adamo, D. W. Shen, C. M. Brooks, J. W. Harter, E. J. Monkman, B. Burganov, D. G. Schlom, and K. M. Shen, *Phys Rev Lett* **110**, 087004 (2013).
- ⁴² S. N. Bushmeleva, V. Y. Pomjakushin, E. V. Pomjakushina, D. V. Sheptyakov, and A. M. Balagurov, *J Magn Magn Mater* **305**, 491 (2006).
- ⁴³ K. Maiti and R. Singh, *Phys Rev B* **71**, 161102 (2005).
- ⁴⁴ J. Lee, Y. Lee, T. Noh, K. Char, J. Park, S.-J. Oh, J.-H. Park, C. Eom, T. Takeda, and R. Kanno, *Phys Rev B* **64**, 245107 (2001).
- ⁴⁵ C. Etz, I. Maznichenko, D. Böttcher, J. Henk, A. Yaresko, W. Hergert, I. Mazin, I. Mertig, and A. Ernst, *Phys Rev B* **86**, 064441 (2012).
- ⁴⁶ P. Vinet, J. H. Rose, J. Ferrante, and J. R. Smith, *J Phys-Condens Mat* **1**, 1941 (1989).
- ⁴⁷ J. Hamlin, S. Deemyad, J. Schilling, M. Jacobsen, R. Kumar, A. Cornelius, G. Cao, and J. Neumeier, *Phys Rev B* **76**, 014432 (2007).
- ⁴⁸ M. Gu, Q. Xie, X. Shen, R. Xie, J. Wang, G. Tang, D. Wu, G. P. Zhang, and X. S. Wu, *Phys Rev Lett* **109**, 157003 (2012).
- ⁴⁹ M. Takizawa, D. Toyota, H. Wadati, A. Chikamatsu, H. Kumigashira, A. Fujimori, M. Oshima, Z. Fang, M. Lippmaa, M. Kawasaki, et al., *Phys Rev B* **72**, 060404 (2005).
- ⁵⁰ D. Toyota, I. Ohkubo, H. Kumigashira, M. Oshima, T. Ohnishi, M. Lippmaa, M. Takizawa, A. Fujimori, K. Ono, M. Kawasaki, et al., *Appl Phys Lett* **87**, 162508 (2005).
- ⁵¹ C. Alexander, S. McCall, P. Schlottmann, J. Crow, and G. Cao, *Phys Rev B* **72**, 024415 (2005).
- ⁵² P. B. Allen, H. Berger, O. Chauvet, L. Forro, T. Jarlborg, A. Junod, B. Revaz, and G. Santi, *Phys Rev B* **53**, 4393 (1996).
- ⁵³ J. Okamoto, T. Mizokawa, A. Fujimori, I. Hase, M. Nohara, H. Takagi, Y. Takeda, and M. Takano, *Phys Rev B* **60**, 2281 (1999).
- ⁵⁴ G.-Q. Liu, V. N. Antonov, O. Jepsen, and O. K. Andersen, *Phys Rev Lett* **101**, 026408 (2008).
- ⁵⁵ J. J. Yeh and I. Lindau, *Atomic Data and Nuclear Data Tables* **32**, 1 (1985).
- ⁵⁶ A. J. Grutter, F. J. Wong, E. Arenholz, A. Vailionis, and Y. Suzuki, *Phys Rev B* **85**, 134429 (2012).
- ⁵⁷ I. V. Solovyev, *J Magn Magn Mater* **177-181**, 811 (1998).
- ⁵⁸ B. T. Thole, P. Carra, F. Sette, and G. van der Laan, *Phys Rev Lett* **68**, 1943 (1992).
- ⁵⁹ J. Rusz, S. Rubino, O. Eriksson, P. M. Oppeneer, and K. Leifer, *Phys Rev B* **84**, 064444 (2011).
- ⁶⁰ J. Verbeeck, H. Tian, and P. Schattschneider, *Nature* **467**, 301 (2010).
- ⁶¹ D. Treves, *Phys Rev* **125**, 1843 (1962).
- ⁶² I. V. Solovyev, *Phys Rev B* **55**, 8060 (1997).
- ⁶³ H. Dürr and G. van der Laan, *Phys Rev B* **54**, R760 (1996).
- ⁶⁴ A fully non-collinear calculation was done with the Elk code, <http://elk.sourceforge.net>. Showing a tilting of 3 deg for the experimental volume with the LDA functional by von Barth and Hedin. The reason the tilting is not larger is that the Ru d-shell is close to half filling, hence the coupling between spin and orbital moment is considerably smaller than the exchange coupling.
- ⁶⁵ F. Bultmark, F. Cricchio, O. Grånäs, and L. Nordström, *Phys Rev B* **80**, 035121 (2009).
- ⁶⁶ P. Bruno, *Phys Rev B* **39**, 865 (1989).